# Contents

# Order and Segmental Mobility in Crystallizing Polymers

A. Nogales[1], A. Sanz[1], I. Šics[2], M.C. García-Gutiérrez[1], and T.A. Ezquerra[1]

[1] Department of Chemistry and Technology of Polymers, Cracow University of Technology, ul. WarszawInstituto de Estructura de la Materia, C.S.I.C. Serrano 119, Madrid 28006, Spain.
[2] Department of Chemistry, State University of New York at Stony Brook, Stony Brook, NY 11794-3400, USA.
imte155@iem.cfmac.csic.es

**Summary.** The simultaneous combination of scattering techniques, probing structure, with relaxation techniques, detecting modifications of the amorphous phase dynamics, can be helpful in order to obtain complementary information about crystallization processes in polar polymers. The objective of this contribution is to review the improvements in the combination of real time (wide and small angle) X-ray scattering and dielectric spectroscopy aiming at a better understanding of polymer crystallization.

## 1 Introduction

Upon cooling liquid systems either crystallize or vitrify or both. From the liquid state, as temperature decreases, the specific volume of a material decreases linearly with temperature (Fig.1). Below the equilibrium melting temperature, $T_m^0$ the liquid is in the (SCL). If temperature is further decreased the specific volume of the supercooled liquid decreases in the same fashion as in the liquid phase. At the glass transition temperature, $T_g$, a change in the slope of the specific volume versus temperature dependence is observed marking the glass transition[1]. An important thermodynamical characteristic of the SCL in the temperature window defined by $T_g$ and $T_m^0$ is that it is unstable due its higher free energy as compared with that of the crystal. Therefore there exists the probability that the supercooled liquid tends to reduce its free energy undergoing a first order phase transition as schematically represented in Fig.1 by the arrow.

This transition by which molecules self-assemble forming crystals is referred to as crystallization [2, 3]. In this case a discontinuous change in the specific volume is expected (Fig.1). A classical experimental approach to characterize the nature of the crystals and the overall fraction of crystalline phase

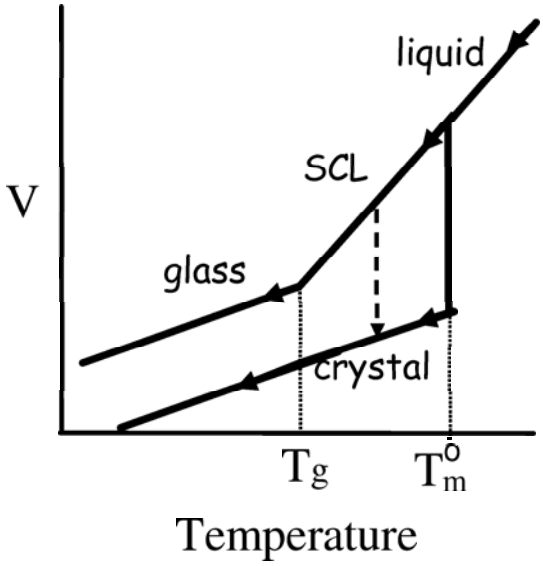


**Fig. 1.** Schematic dependence of the specific volume (V) of a given material as a function of temperature indicating the liquid, super cooled liquid (SCL), glassy and crystalline state.

mainly involves scattering and diffraction measurements [4]. Precise information about the changes occurring in supercooled liquids upon crystallization can be obtained when a real time experimental set up is used [5–7]. Nowadays, as far as crystalline phase development is concerned, both synchrotron and neutron sources offer the possibility to perform real time diffraction experiments [6, 8].

As an example, fig. 2a shows the evolution with temperature of the neutron diffraction patterns of isopropanol upon heating. Here, isopropanol was quenched from the liquid state to avoid crystallization upon cooling [6, 7]. As temperature increases the initial SCL exhibits the diffraction pattern characteristics of an amorphous system. Upon heating from the SCL state isopropanol crystallizes and the diffraction pattern presents narrow Bragg peaks characteristic of a crystalline phase. Further heating above the melting temperature produces a crystal destruction and the characteristic diffraction pattern of an amorphous system, now the liquid phase, is recovered. Scattering techniques can also be used to extract structural information in amorphous materials [9]. However, due to the fact that crystals provoke strong diffraction phenomena, superimposed over a relatively weak contribution of the amorphous phase, mainly information about the crystalline phase is obtained.

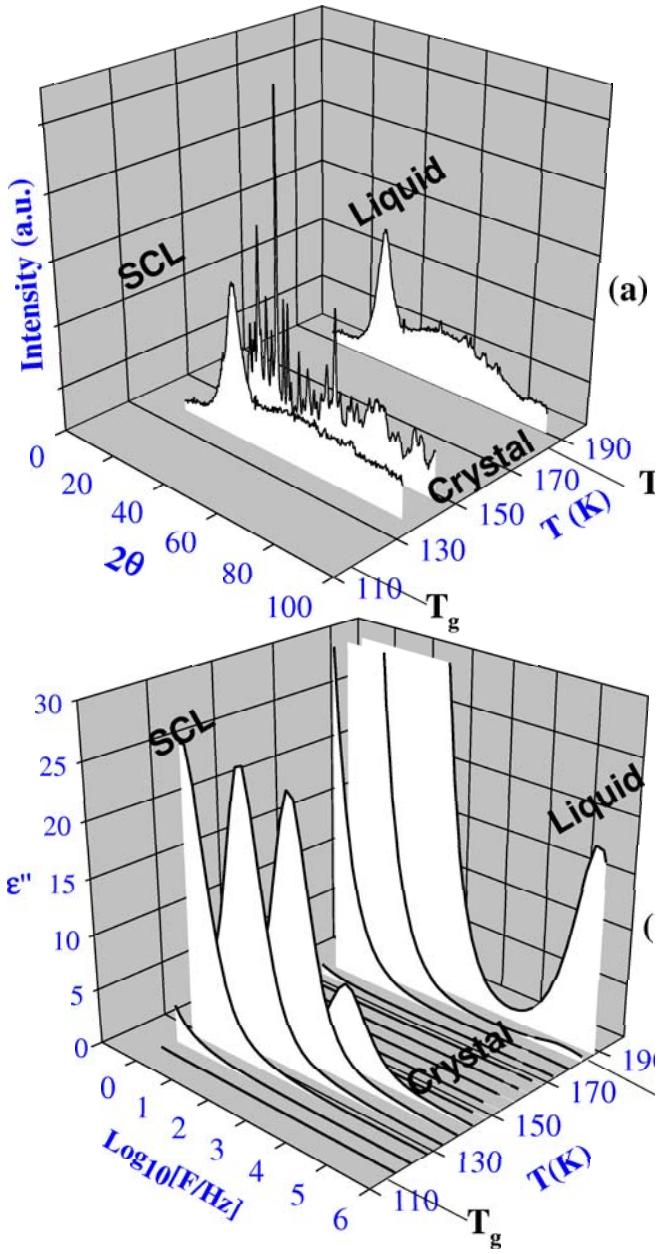


**Fig. 2.** (a)Evolution with temperature of the neutron diffraction patterns of isopropanol. Both in the liquid and in the super cooled liquid state(SCL) the diffraction patterns are characteristic of an amorphous material. The crystalline state presents characteristic narrow Bragg peaks of a crystalline phase. (b)Evolution with temperature of the main relaxation of isopropanol. Molecular mobility at $T>T_g$ is revealed by the main relaxation of isopropanol as reflected by the maximum in frequency of the imaginary part, $\epsilon''$, of the complex dielectric permittivity. The main relaxation appears in both the super-cooled and the liquid state. However, in the crystalline state, where no significant molecular mobility is expected, the relaxation vanishes [6, 7]. Isopropanol was quenched from the liquid to the glassy state.

Thus, processes occuring in the amorphous fraction during crystallization of the supercooled liquid are almost non-detectable for these techniques due to the absence of order. An improvement in the understanding of crystallization in terms of interrelation between crystalline and amorphous development is obtained when diffraction experiments are simultaneously accompanied by (DS) [10, 11]. At $T>T_g$ molecular mobility in liquids and segmental mobility in polymers is revealed by the which appears as a maximum in frequency of the imaginary part, $\epsilon''$, of the complex dielectric permittivity [12]. Regarding the amorphous phase, it has been shown that, upon crystallization, the $\alpha$ relaxation, which is related to the segmental dynamics, can be used as a probe for crystallization because it is strongly affected by the progressive development of the crystalline phase [13–17]. As an example, fig. 2b shows the evolution with temperature of the main relaxation of isopropanol. This maximum observed in both the supercooled and the liquid state appears as a consequence of the molecular mobility about $T_g$. Accordingly, in the crystalline state, where no significant molecular mobility is expected, the relaxation vanishes [6, 7].

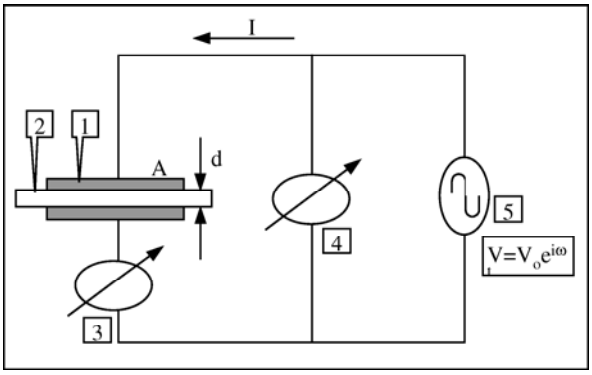


**Fig. 3.** Schematic view of a typical dielectric spectroscopy experiment. (1) Electrodes of area A, (2) Sample film of thickness d, (3) Current Analyzer, (4) Voltage Analyzer, (5) Alternating Voltage generator.

Therefore by monitoring simultaneously in real time the crystal development, by means of diffraction techniques, and the dynamic changes occurring in the amorphous phase, by means of dielectric spectroscopy, a complete picture of the crystallization process could be obtained. Among the glass forming systems, high molecular weight polymers, tend to develop a characteristic folded chain crystalline lamellar morphology at the nanometer level upon ther-

mal treatment within the temperature range defined between $T_g$ and $T_m^0$ [3]. The lamellar morphology consists of stacks of laminar crystals and amorphous regions intercalated between them. Although extended chain crystals are thermodynamically more stable, a kinetic factor induces that a polymer chain folds several times, building up thin crystal lamellae. For semicrystalline polymers, this characteristic crystalline nanostructure acts as an internal backbone in the polymer controlling the final mechanical properties of the material.

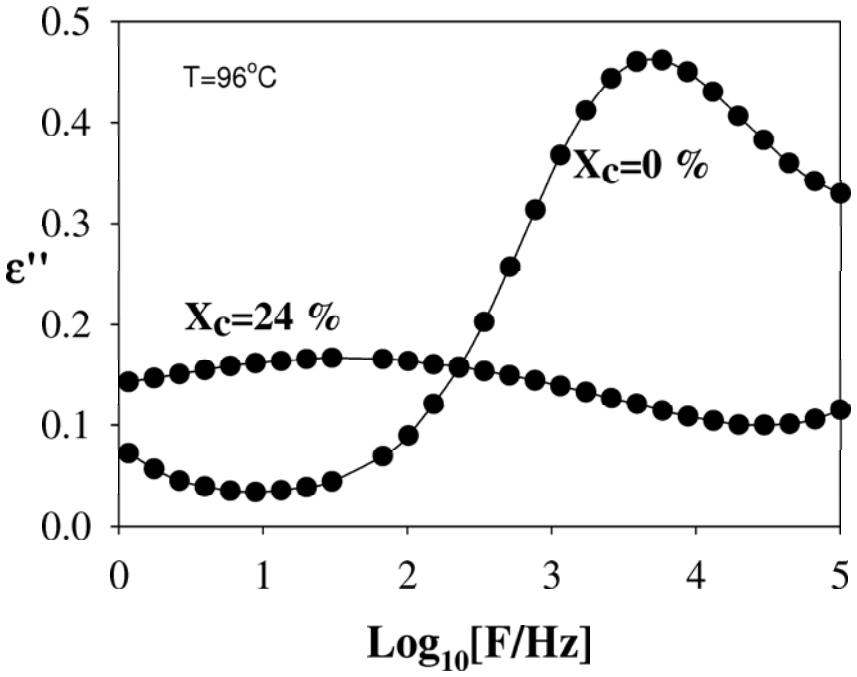


**Fig. 4.** Dielectric loss, $\epsilon''$, as a function of frequency, F=$\omega/(2\pi)$, for amorphous PET (crystallinity $X_c$=0) and semicrystalline ($X_c$=24 %)PET at T=96°C.

The objective of this contribution is to review the improvements in the combined use of real time X-ray scattering and dielectric relaxation techniques experiments for a better understanding of polymer crystallization.

## 2 Description of the experimental set-up for simultaneous Small and Wide angle X-ray Scattering and Dielectric Spectroscopy(SWD)

Dielectric spectroscopy is a technique which allows one to evaluate the complex dielectric permittivity $\epsilon^* = \epsilon' - i\epsilon''$ as a function of frequency and temperature, where $\epsilon'$ is the dielectric constant and $\epsilon''$ is the dielectric loss [3, 12]. A schematic view of a dielectric spectroscopy experiment is shown in fig. 3. A dielectric sample of thickness $d$ and area $A$ is subjected to an alternating electric field of angular frequency $\omega$. Through measurements of the complex impedance of the sample it is possible to experimentally determine $\epsilon^*$ [12, 18–20]. Dielectric spectroscopy is a very suitable method to study molecular dynamics in polymers above $T_g$. In this case, segmental motions of the polymeric chains give rise to the so called $\alpha$-relaxation process, which can be observed as a maximum in $\epsilon''$ and a step-like behavior in $\epsilon'$ as a function of frequency. Both, the intensity of the $\alpha$ relaxation, $\epsilon''_{max}$, and the frequency of maximum loss, $F_{max}$, are very sensitive to crystallinity, which produces a decrease in $\epsilon''_{max}$ and a shift of $F_{max}$ towards lower values when crystallization proceeds [13–17]. This behavior is illustrated in fig. 4 for poly(ethylene terephthalate)(PET). Crystallisable polymers tend to develop a certain level of crystallinity provided they are heated at temperatures above the glass transition temperature. The microstructure of semicrystalline polymers typically shows a distinct lamellar morphology consisting of stacks of laminar crystals intercalated by amorphous less ordered regions. The lamellar stacks are characterized by the thickness of the crystals ($l_c$) and that of the amorphous layers ($l_a$). Both characteristic lengths define the long period as $L=l_a+l_c$ which can be experimentally determined through small angle X-ray scattering experiments (SAXS) [3, 21]. The $X_c$ can be estimated experimentally from Wide Angle X-ray Scattering measurements (WAXS).

In recent times there have been different works reporting dielectric environments useful to accommodate simultaneous X-ray experiments [10, 22, 23] . A typical scheme of a SAXS-WAXS-DS sample holder (SWD), is illustrated in fig. 5. The sample (1) is placed between two metallic disks (3) acting as electrodes. These are electrically insulated by polyamide films (5) from the heating blocks (4). Heating power is provided by some heating-elements (6) embedded in the sample-cell heating blocks (4). In order to allow the passage of the X-ray beam through the sample, central holes were machined in both, the electrodes and in the heating blocks. The sample, prepared in the form of a film, can be provided with thin circular gold electrodes by sputtering the metal in both free surfaces. The sample film was sandwiched between two thin aluminium disks (2) in order to provide homogeneous heating for the whole sample surface. The sandwich is placed in between the two metallic electrodes (3). Cooling of the device can be obtained by compressed air circulating through a metallic pipe (7) embedded in one of the sample-cell heating blocks. A thermometer (8) is located in one of the metallic electrodes. Elec-

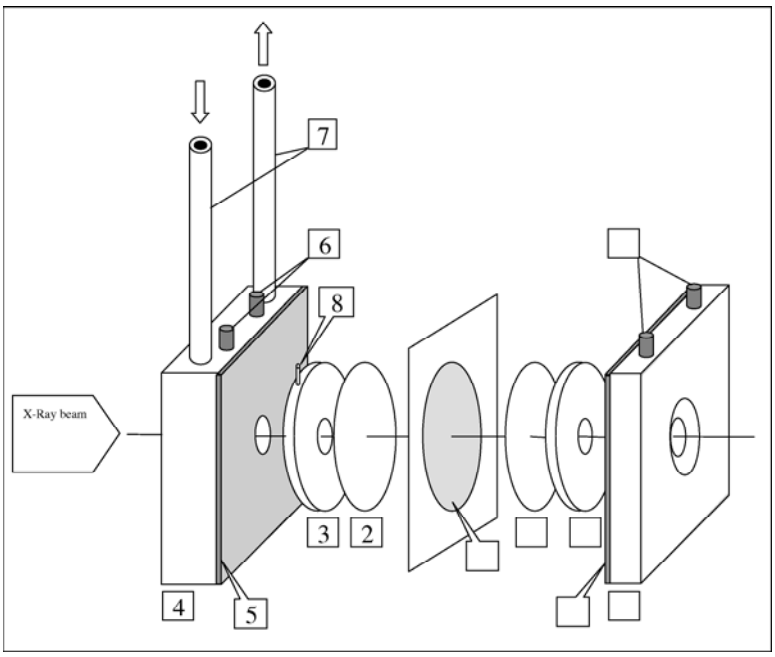


**Fig. 5.** Scheme of the SAXS-WAXS-DS cell. (1) Sample, (2) Aluminum disks, (3) Electrodes, (4) Heating blocks, (5) Insulating polyamide film, (6) heating elements, (7) cooling pipes, (8) PT-100 thermometer.

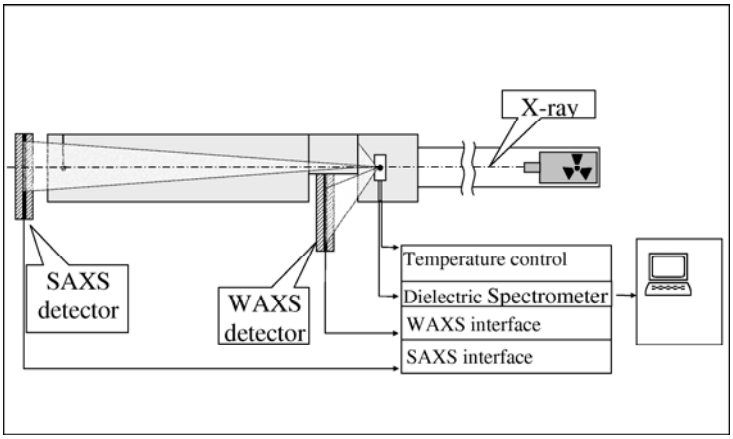


**Fig. 6.** Scheme of a typical experimental set-up for simultaneous SAXS-WAXS-DS experiments at a polymer beam-line.

trodes can be connected to a suitable dielectric spectrometer to measure ($\epsilon^*$) in a convenient frequency range [10]. These kind of cells, where simultaneous WAXS and SAXS measurements are performed, can be easily incorporated into a typical synchrotron beam line [10, 23] using two position sensitive detectors as presented in fig. 6. Closer to the sample, the WAXS detector is positioned off the primary beam allowing the SAXS intensity to pass above and to be measured by the SAXS detector located at a larger distance.

## 3 Dielectric relaxation of amorphous polymers: Poly(ethylene terephthalate)

Poly(ethylene terephthalate)(PET) is one of the most common polymers provided by the polymer industry for fiber and packaging purposes [24]. As far as polymer crystallization is concerned, PET can be considered as a paradigm of a crystallisable polymer due to the fact that PET can be obtained either in the amorphous state or with a controlled amount of crystallinity. Therefore, PET has been used to study the influence of crystallinity in a great variety of physical properties including thermal behavior [16, 25–29], structure development [30–33] and mechanical and dielectric behavior among others [13, 14, 34, 35]. Fig.7 presents the dielectric loss, $\epsilon''$, and dielectric constant, $\epsilon$', for amorphous PET at T>T$_g$ as a function of frequency for different temperatures.

Amorphous PET (Rhodia S80 from RhodiaSter, $M_\nu$=45000 g/mol) was prepared by quenching from the molten state as described elsewhere [35]. Broad-band dielectric spectroscopy measurements of the complex dielectric permittivity were performed from $10^{-1}$ Hz to $10^6$ Hz by using a BDS-40 Novocontrol system and from $10^6$ Hz to $10^9$ Hz by means of a Novocontrol BDS-60 coaxial line reflectometer. The broad-band data show the $\alpha$-relaxation process, at lower frequencies, and the subglass $\beta$-relaxation process at higher frequencies. As extensively reported [12], the relaxations manifest themselves as maxima in $\epsilon$" and concurrent steps in $\epsilon$'. As the temperature increases the frequencies of maximum loss, $F_{max}$, shift towards higher values. At low frequencies the relaxations are accompanied by a strong increase of $\epsilon$" corresponding to a dc-conductivity contribution. Isothermal $\epsilon$" and $\epsilon$' data can be phenomenologically described according to the Havriliak-Negami equation [12, 14, 36] given by:

$$\epsilon^* = \sum_{x=\alpha,\beta} \frac{(\epsilon_0 - \epsilon_\infty)_x}{[1 + (i\omega\tau_x)^{b_x}]^{c_x}} + (\epsilon_\infty)_\beta - i\frac{\sigma}{\epsilon_{vac}\omega^s} \qquad (1)$$

where $\omega = 2\pi F$, $\epsilon_0$ and $\epsilon_\infty$ are the relaxed ($\omega$=0) and unrelaxed ($\omega$=$\infty$) dielectric constant values, $\tau$ is the central relaxation time of the and $b$ and $c$ (0<b,c<1) are shape parameters which describe the symmetric and asymmetric broadening of the relaxation time distribution function, respectively [36].

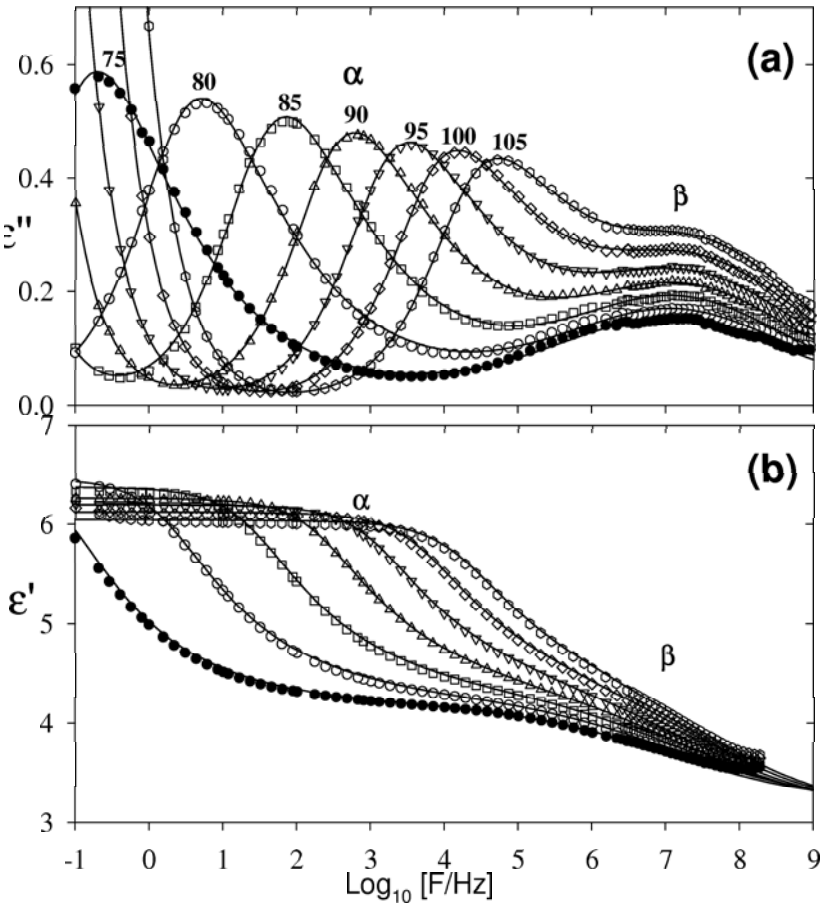


**Fig. 7.** Amorphous PET: (a)dielectric loss,$\epsilon$" and (b) dielectric constant, $\epsilon$', as a function of frequency for different temperatures labelled in °C.

The subscript makes reference either to the $\alpha$ or the $\beta$ relaxation. The last term of eq.1 corresponds to the conductivity contribution. Here, $\sigma$ is related to the direct current electrical conductivity, $\epsilon_{vac}$ is the vacuum dielectric constant and $s$ depends on the nature of the conduction mechanism. The results from this phenomenological data analysis are presented in fig.7 by the continuous curves. Amorphous PET presents an strongly asymmetric $\alpha$-relaxation as denoted by an asymmetric broadening parameter c=0.4 nearly constant in the studied temperature range [35]. On the contrary, the $\beta$-relaxation is symmetric, c=1, in the presented temperature range. The central relaxation

time, $\tau$, for the $\beta$ process follows an Arrhenius behavior characteristic of a non-cooperative process [14] with an activation energy of about 13 Kcal/mol. The origin of the subglass relaxation has been traditionally associated to the local motion of the ester group [14] although recent dielectric measurements indicate a more complex molecular origin [37, 38]. The $\alpha$-relaxation appears as a consequence of the segmental motions of the amorphous phase above the glass transition temperature and the temperature dependence of its relaxation time can be described by means of the Vogel-Fulcher-Tamann (VFT) [3, 12].

## 4 Time resolved cold crystallization by SWD

### 4.1 Poly(ethylene terephthalate)

Fig.8 shows an experiment for PET. SAXS,WAXS and DS data have been simultaneously collected during a cold crystallization experiment at $T_c$ = 96°C and are shown for three different crystallization times during the crystallization process. Each set of measurements was collected during 60 s. The experiments were performed in the Soft Condensed Matter beam-line A2 at HASYLAB in the synchrotron facility DESY in Hamburg ,Germany. Both, WAXS and Lorentz corrected SAXS intensities [21] are represented as a function of the scattering vector s=$(2/\lambda)\sin(\theta)$ being $2\theta$ the scattering angle and $\lambda$ =0.15nm the wavelength of the X-ray used. Complex dielectric permittivity measurements were performed in the frequency range of $10^1$ Hz<F<$10^5$ Hz, using a Novocontrol system integrating a SR 830 Lock-in amplifier with a BDC-L dielectric interface. The dielectric loss data, $\epsilon$" are given as a function of frequency. The initial amorphous state is characterized by a broad halo in the WAXS pattern, a continuous scattering in the SAXS pattern and a relaxation process characterized as a maximum in $\epsilon$" centered around a $F_{max}$ value of $\approx$ 4x$10^3$ Hz. The observed relaxation can be identified with the $\alpha$ process. As time increases, the onset of crystallization manifests itself by the appearance of the characteristic Bragg peaks of the triclinic unit cell of PET in the WAXS patterns. The weight fraction index of crystallinity ($X_c$ ) can be estimated from the ratio between the area below the crystalline Bragg peaks to the total scattered area after appropriate subtraction of a flat background [39]. Dashed lines in fig.8 illustrate the peak deconvolution procedure. In the SAXS patterns an increase of the scattered intensity at lower s-values that develops into a well defined peak centered around a value of s=0.125 $nm^{-1}$ is observed. This fact indicates that lamellar crystals organize themselves forming lamellar stacks with an average distance between gravity centers of consecutive lamellar crystals of L=$1/s_{max}$ $\approx$8 nm. The structural features are accompanied by changes in the dynamics of the amorphous phase as revealed by the simultaneous DS experiment. The $\alpha$-relaxation exhibits, at the end of crystallization, a decrease in its intensity and a shift towards lower values of its $F_{max}$. At intermediate crystallization times a significant broadening in the low frequency

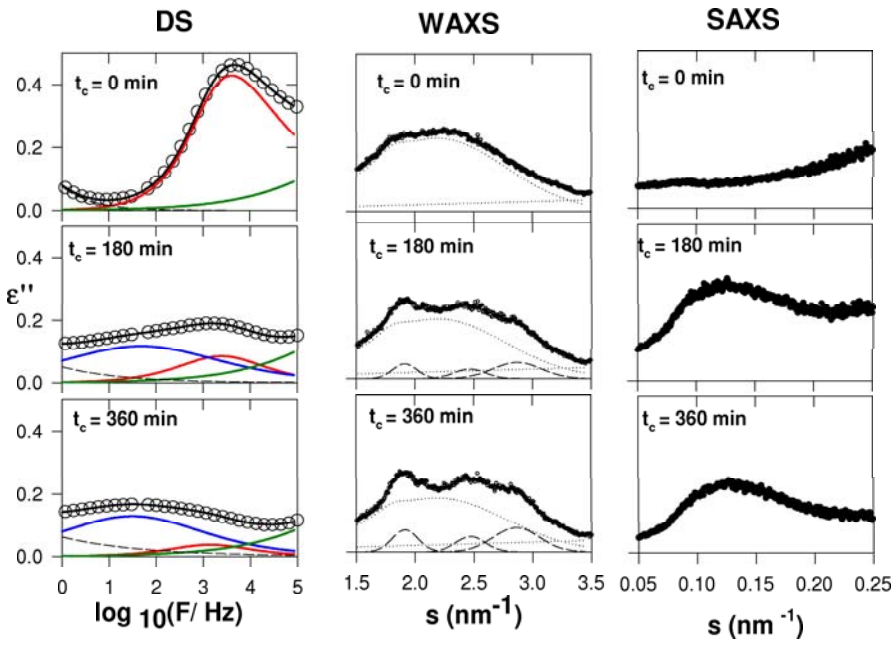


**Fig. 8.** Simultaneous dielectric loss, $\epsilon$", WAXS and, SAXS experiments during crystallization of initially amorphous PET at $T_c$=96°C for three different crystallization times covering the crystallization process. Continuous lines in the DS-data indicate the separate contribution of the primary and secondary $\alpha$-relaxations, the $\beta$-relaxation tail appearing at higher frequencies and the conductivity tail appearing at lower frequencies. Dotted and dashed lines in the WAXS-data illustrate the peak deconvolution procedure.

side of the relaxation is detected. This effect can be described as an additional $\alpha'$-process appearing as crystallinity develops [22, 35]. The dielectric data can be analyzed in terms of the HN-equation considering the contribution of i) the initial $\alpha$-process ; ii) the second appearing during crystallization iii) the $\beta$-relaxation process which contributes in the higher frequency range of the spectrum and iv) the conductivity which influences the lower frequency part of the spectrum [35]. The separate contribution of every process as well as the total fittings are represented in fig.8 by the continuous lines. A visualization of the changes in the characteristic parameters simultaneously measured is presented in fig.9. In this figure we have represented as a function of the crystallization time for both the initial $\alpha$ and the secondary $\alpha$'-relaxation processes: (a) The dielectric strength, (b) the broadening parameter (c) the asymmetry parameter (d) the central relaxation time. Additionally values for

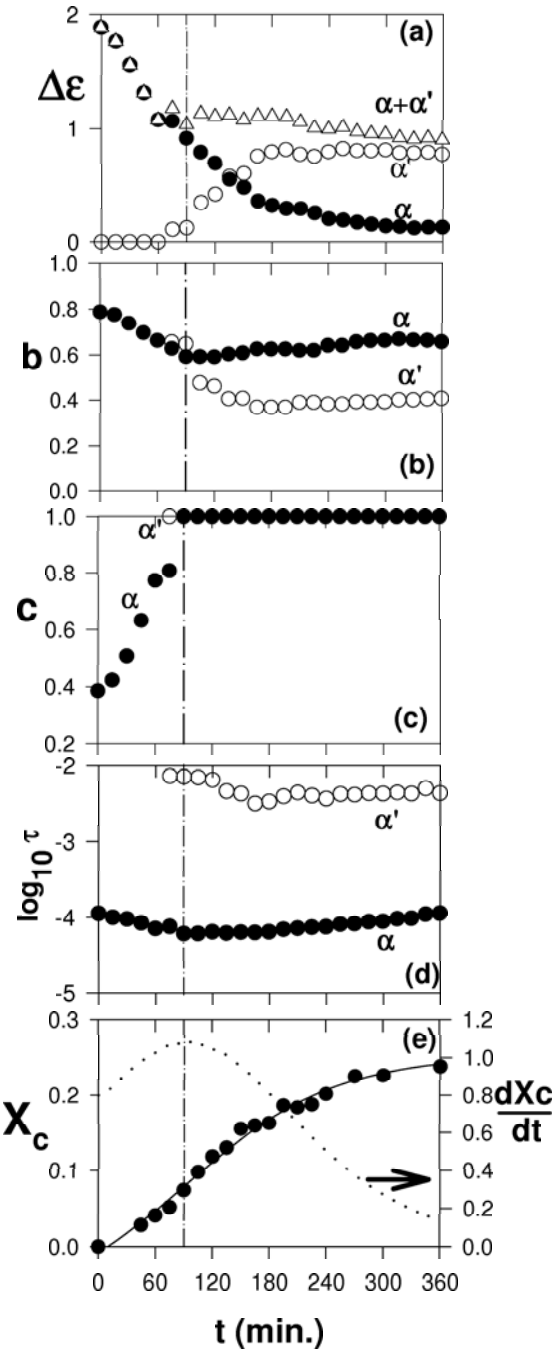


**Fig. 9.** Summary of physical parameters obtained from the SWD experiment for PET at T=96°C as a function of the crystallization time: (a) (•)$\Delta\epsilon$ values for the $\alpha$ relaxation, (○)$\alpha$' relaxation and (△)$(\Delta\epsilon)_\alpha + (\Delta\epsilon)_{\alpha'}$ . (b) broadening parameter for the (•)$\alpha$ relaxation and (○)$\alpha'$ relaxation (c) Asymmetry parameter for the (•)$\alpha$ relaxation and (○)$\alpha$' relaxation (d) Central relaxation times for the (•)$\alpha$ relaxation ,(○) $\alpha$' relaxation (e) Crystallinity index (left) and slope of the crystallinity curve (right) .

the weight fraction index of crystallinity ($X_c$ ) are included (fig.9 e) calculated from the WAXS data.

From the simultaneous SWD-experiments the following attempt to relate structure and dynamics can be made. For times shorter than a characteristic one (t $\approx$ 90 min) the decrease of $(\Delta\epsilon)_\alpha$, fig.9a, indicates a significant reduction of the mobile material which follows the increase of crystallinity (fig.9e). However, the reduction of $(\Delta\epsilon)_\alpha$ is stronger than the increment in crystallized material as determined by the increase of $X_c$. This effect, observed in different polymers [13, 17], can be attributed to the formation of an frequently referred to as rigid amorphous phase (RAP) [40].

During this initial period of crystallization, in spite of the strong reduction in $(\Delta\epsilon)_\alpha$ of about 50 %, the remaining mobile material, in the amorphous phase, only slightly change the average segmental mobility in the amorphous phase as reflected by the moderate variation observed in $\tau_\alpha$ (fig.9 d). During this initial period the relaxation tends to become symmetric and increasingly broader, as denoted by the increase of the $c_\alpha$-parameter and the decrease of the $b_\alpha$-parameter respectively (fig.9 b and c). As crystallization proceeds above the characteristic time, a secondary relaxation, $\alpha$' , appears at lower frequencies. The fittings indicate that the $\alpha$'-relaxation can be treated in a first approach as a symmetric process ($c_\alpha$'= 1). As crystallization time increases the dielectric strength of the $\alpha$'-relaxation, $(\Delta\epsilon)_\alpha$', increases at expenses of $(\Delta\epsilon)_\alpha$ (fig.9 a). At the end of the crystallization process $(\Delta\epsilon)_\alpha$ tends to vanish and $\alpha$' becomes the characteristic $\alpha$-relaxation of the semi-crystalline material.

### 4.2 Poly(ethylene terephthalate)/Poly(ethylene naphthalene 2,6-dicarboxilate) blends

Blending of poly(ethylene terephthalate) (PET) and poly (ethylene naphthalene -2,6 -dicarboxylate) (PEN) has been shown to be an attractive possibility to combine the inherent economics of PET with the superior mechanical, thermal and barrier properties of PEN [24]. The molecular structure of PEN is stiffer than that of PET due to the presence in its main chain of naphthalene instead of benzene rings. The glass-transition temperature, $T_g$, of PEN is about 50°C higher than that of PET contributing to a better performance in terms of thermal, mechanical, and gas barrier properties [17, 24]. PET and PEN are immiscible polymers that tend to form separated phases upon blending [41]. However, at temperatures above 270 ° C certain amounts of PET-PEN block copolymers develop due to transesterification reactions [41, 42]. By cryogenic grinding, melt pressing at 300 °C and subsequent quenching amorphous films of PET/PEN blends with various degrees of can be prepared [42]. For low levels of transesterification two glass-transition steps, two peaks of crystallization and melting and two $\alpha$-relaxation processes are observed indicating the existence of a phase separated system consisting on different PET-rich and PEN-rich phases [42].Figure 10 displays the imaginary part

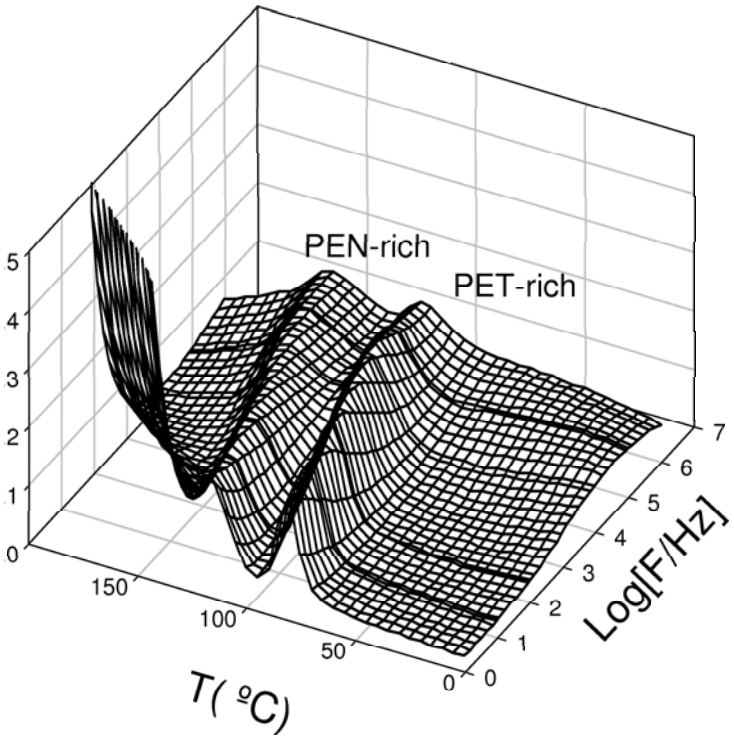


**Fig. 10.** Frequency and temperature dependence of $\epsilon$" for a 56:44 mol % PET/PEN blend prepared by cryogenic grinding, pressed at 300°C for 3 min and quenched on ice-water.Fraction of T-E-N triads: 11 %.

$\epsilon$" of the dielectric permittivity $\epsilon^*$ as a function of frequency and temperature for a PET/PEN (56:44 molar ratio, corresponding to 1/1 in weight) pressed for 3 min at 300°C. The degree of transesterification ($f_{TEN}$), as estimated, from $^1$H NMR, by the fraction of terephthalate-ethylene-naphthalene-2,6-dicarboxylate triads (T-E-N) is for this sample of $f_{TEN}$=11 % [42, 43]. In fig.10 one can distinguish two $\alpha$-processes associated with the glass transitions in PET-rich and PEN-rich regions, respectively [42]. Atomic Force Microscope (AFM) studies in samples with low levels of transesterification reveal the presence of PET domains typically smaller than 50 nm well dispersed without significant clustering [43]. The confinement of PET within these phase segregated domains is expected to have a strong influence on its crystallization behaviour. The crystallization of polymers in confined environments is a topic of permanent interest because it can be useful to better understand the transition from random coil chains to ordered lamellae which takes place during crystallization [44]. Figure 11 shows the time-resolved SAXS-WAXS-

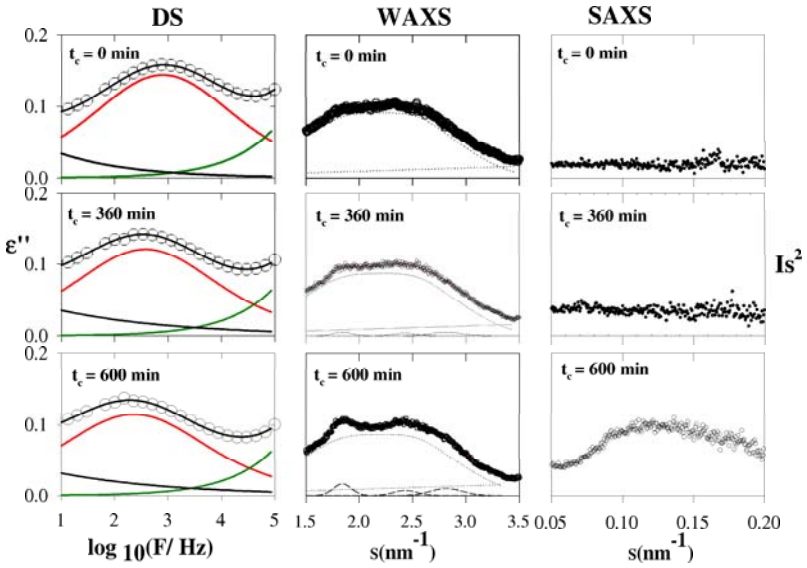


**Fig. 11.** Simultaneous dielectric loss,$\epsilon$", WAXS and, SAXS experiments during crystallization of initially amorphous PET/PEN blends (1:1 by weight) with a $f_{TEN}$ =11 % at $T_c$=96° C for three selected crystallization times. Continuous lines in the DS-data indicate the separate contribution of the $\alpha$-relaxation, the $\beta$-relaxation tail appearing at higher frequencies and the conductivity tail appearing at lower frequencies. Dotted and dashed lines in the WAXS-data illustrate the peak deconvolution procedure.

DS data simultaneously collected during a cold crystallization experiment of a 1:1 by weight PET/PEN blend with $f_{TEN}$=11 % at $T_c$ = 96° C for three selected crystallization times. The PEN is from Eastman with $M_\nu$= 25 000 g/mol. By comparison with the crystallization of pure PET ( fig.8), here the crystallization kinetics is significantly slower. However, similarly to what it was previously shown for PET, for this PET/PEN sample lamellar crystals organize themselves forming a nanostructure of lamellar stacks with an average distance between gravity centres of consecutive lamellar crystals of about 8 nm. The $\alpha$-relaxation exhibits, at the end of crystallization, a decrease in its intensity and a shift towards lower values of $F_{max}$. In contrast with the case for pure PET, now the dielectric data can be described by means of a superposition of a single $\alpha$-process in addition to the $\beta$-relaxation process which contributes in the higher frequency range of the spectrum and the conductivity which influences the lower frequency part of the spectrum [45]. The separate contributions of every process as well as the total fittings are represented in fig.11 by the continuous lines. The selected crystallization temperature is well

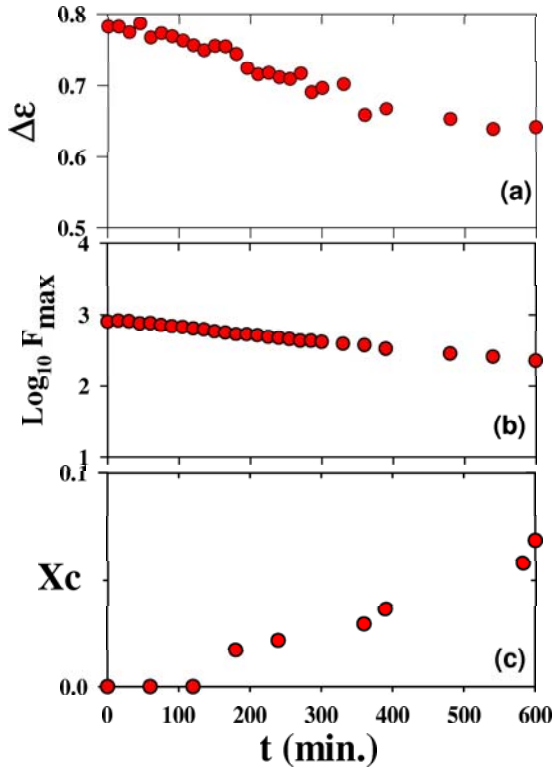


**Fig. 12.** Summary of parameters from the SWD experiment for PET/PEN blends (1:1 by weight) with $f_{TEN}$ =11% at $T_c$=96°C as a function of the crystallization time: (a)$\Delta\epsilon$ values for the $\alpha$-relaxation, (b) Frequency of maximum loss, (c) Crystallinity index , $X_c$ .

below the calorimetric $T_g$ of PEN. Therefore the influence of the $\alpha$-relaxation of PEN [46] on the low frequency contribution of the DS experiments can be discarded. Figure 12 presents the characteristic parameters of the $\alpha$-relaxation as a function of the crystallization time including the dielectric strength and the frequency of maximum loss which in this case corresponds to $(2\pi\tau_\alpha)^{-1}$. Additionally, values for the weight fraction index of crystallinity ($X_c$ ) are included calculated from the WAXS data. In this case ( $f_{TEN}$ =11% ), after considering the PET/PEN weight ratio, the final crystallinity of PET is comparable with that reached in pure PET. However a significant slowing down of the PET crystallization with transesterification, as compared with that of pure PET, is evident. During crystallization at T=96 °C, there is reduction of the mobile material, reflected by the decrease of $\Delta\epsilon$ (fig.12a) which

is accompanied by an increase of crystallinity (fig. 12c). During crystallization, the remaining mobile material reduces its average segmental mobility in the amorphous phase as reflected by the decrease of $F_{max}$ with crystallization time (Fig.12b) and the shape of the $\alpha$-relaxation remains essentially constant. This behaviour is in contrast with that observed under similar conditions for pure PET.

## 5 Development of the rigid amorphous phase (RAP) as revealed by SWD

### 5.1 Aromatic Polyesters: Poly(ethylene terephthalate), Poly(butylene isophthalate)

The above features, which emerge directly from the simultaneous SAXS, WAXS and DS experiments enable us to propose the following explanation for the cold crystallization of PET. During the initial stages of the process, before the characteristic time, lamellar crystals develop involving a strong formation of rigid amorphous phase as revealed by the increase observed in $X_c$ and the decrease of $(\Delta\epsilon)_\alpha$. In this regime, the average mobility of the remaining mobile amorphous phase is slightly affected, as revealed by the small variation with time of $\tau_\alpha$. One possibility to explain these features is that the amorphous regions located between consecutive crystals within the lamellar stack become immobilized as soon as the lamellar stack is formed during the initial stages of crystallization before the characteristic time. This could explain the strong reduction of $\Delta\epsilon$ for moderate increase of $X_c$. A similar view was recently proposed to explain oxygen transport properties of PET [47]. In fact, oxygen permeation measurements indicate that the amorphous region within the lamellar stacks can be associated with the rigid amorphous phase (RAP). Moreover, recent AFM observations of the PET indicate that molecular mobility in these regions should be strongly inhibited [48]. Accordingly, in this initial stage, the $\alpha$-relaxation should predominantly originate in the inter-lamellar stacks amorphous regions. Around the characteristic time a significantly slower process appears, the $\alpha$'-relaxation. Due to the fact that in the present case cold crystallization takes place relatively close to $T_g$ the crystallinity evolution spreads in time. Thus, the transition from primary to secondary crystallization regimes is not so well defined as for crystallization at higher temperatures. By calculating the slope of $X_c$ with time, continuous line referred to the right y-axis in fig.9e, it is observed that the characteristic time at which the secondary $\alpha$-relaxation starts to appear is close to the inflexion point of the crystallinity curve. This inflexion point can be associated to the moment in which significant impingement of lamellar stacks may locally occur during primary crystallization. After impingement, secondary crystals are likely to develop. This suggests that secondary crystals growing in the inter-lamellar stacks amorphous phase may act as physical cross-links tending to

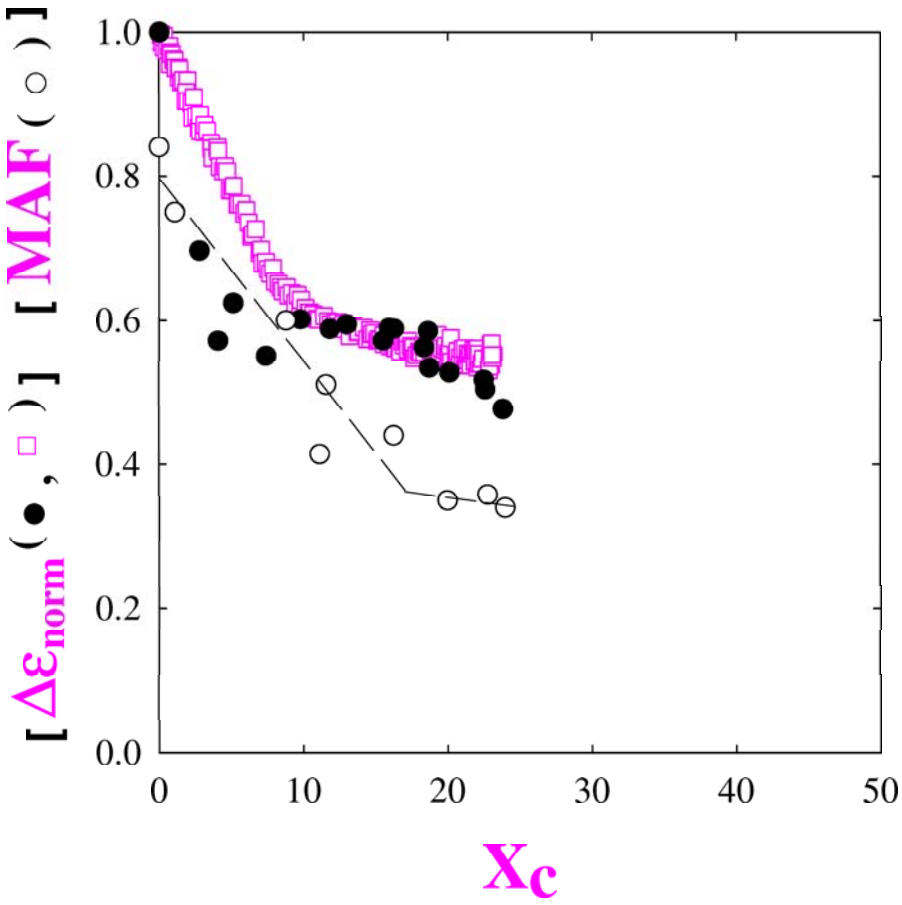


**Fig. 13.** Normalized dielectric strength $(\Delta\epsilon)_{norm}$ as a function of the crystallinity $X_c$ for:(•)PET crystalized at T=96°C (SWD-data).(□)Poly(butylene isophthalate)(PBI)crystallized at T=60°C(SWD-data[49]). (○)Mobile Amorphous Fraction (MAF)(calorimetry data) for PET crystallized at T=117°C (data extracted from fig.3 of ref.[29]

slow-down segmental dynamics and giving rise to the secondary $\alpha$-relaxation, $\alpha'$. The influence of different crystallization regimes on the dynamics is further emphasized in fig.13. In that plot, $\Delta\epsilon$ values for PET, normalized to its initial value, are presented versus crystallinity. $\Delta\epsilon_{norm}$ can be considered as a measure of the fraction of relaxing species and therefore representative of the mobile amorphous fraction (MAF). As observed in fig.13, $\Delta\epsilon_{norm}$ decreases with $X_c$ exhibiting two clear tendencies. Initially, $\Delta\epsilon_{norm}$ presents a slope far away from -1, indicating that during initial crystallization the immobilized

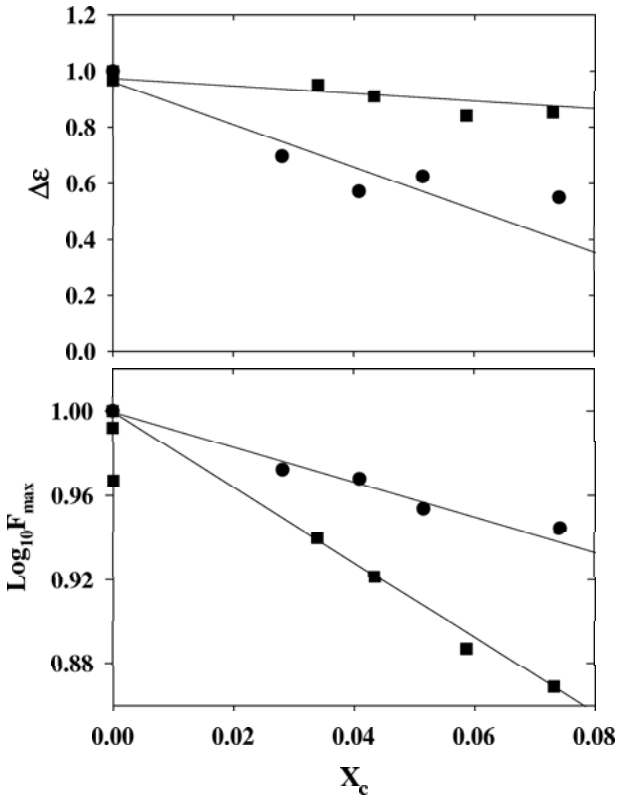


**Fig. 14.** Evolution of normalized $\Delta\epsilon$ and $F_{max}$ values with crystallinity during an SWD isothermal crystallization experiment at T=96°C for both PET (•) and PET/PEN 1:1 by weight with $f_{TEN}$ =11% (■). The crystallinity values for the PET/PEN blend have been corrected by the weight concentration.

segments are not only those included in the crystals but also a certain portion of the non-crystallized segments corresponding to the rigid amorphous phase (RAP). For $X_c$ higher than $\approx 10$ % the tendency of $\Delta\epsilon_{norm}$ changes drastically and a second slope closer to -1 is observed. This effect can be interpreted assuming that for $X_c > 10\%$ the immobilization of material by RAP formation is not as effective as in the previous period being the amount of immobilized material closer to the amount of material incorporated to the crystals. A rather similar effect has been recently found by calorimetry for PET crystallized at 117 °C [29]. Here, estimates of the mobile amorphous fraction (MAF) could be calculated by measuring the heat capacity increment at the $T_g$. In fig.13 data corresponding to these MAF values have been included for comparison. The existence of two crystallization regimes with two different ratios

of RAP formation is also evident. Similar data have been found by means of SWD for other polymer, namely poly(butylene isophthalate)(PBI)[49], and the corresponding $(\Delta\epsilon)_{norm}$ data are also included in fig.13 for comparison. One may propose the idea that in the second regime, which we can associate with the secondary crystallization, crystallization takes place essentially in the inter lamellar stacks amorphous phase. These secondary crystals should be arranged either as independent lamellae or as very defective stacks. This mechanism should not produce significant amounts of RAP because, as previously discussed, the RAP can be assigned to an intra lamellar stacks amorphous phase. Additional support for this model on the basis of structural experiments has been discussed extensively for PBI [49]. A similar view has been recently proposed to explain secondary crystallization in poly(ethylene isophthalate-co-terephtalate) copolymers crystallized from the melt [50].

### 5.2 Confined crystallization of PET in PET/PEN blends

As mention previously, cryogenic mechanical alloying of PET and PEN, 1:1 by weight, and the subsequent heat treatment followed to obtain films produce a phase separated morphology of PET and PEN rich domains for low levels of transesterification ($f_{TEN}$ = 11%) [42, 43]. In this case, significant crystallization of PET within the PET domains is possible as shown in fig.11. In principle it is difficult to separate the effect of sequence length from those of confinement. However, for low levels of transesterification, the existence of two well defined calorimetric glass transition temperatures [42], and two $\alpha$-relaxations, as revealed by dielectric spectroscopy (fig.10) and by dynamic mechanical analysis [43], indicate that T-E-N linkages are more likely to be located within the interface among PET and PEN phase separated domains. In this case ($f_{TEN}$ =11% ), after consideration of the PET/PEN weight ratio the final crystallinity reached by PET in the PET/PEN blends( fig.11), is comparable with that reached in pure PET (fig.8). However a significant slowing down of the PET crystallization is observed. From the SWD-experiments a relationship between structure and dynamics for PET crystallization in the PET/PEN blends with low transesterification levels can be attempted. During crystallization at T=96°C, there is a reduction of the mobile material, reflected by the decrease of $\Delta\epsilon$ (fig.12a) which, similarly as in the neat PET case (Fig.8), parallels the increase of crystallinity (fig. 12c). During crystallization, the remaining mobile material reduces its average segmental mobility in the amorphous phase as reflected by the decrease of $F_{max}$ with crystallization time (Fig. 12b) while the shape of the $\alpha$-relaxation remains essentially constant. This behaviour is in contrast with that observed under similar conditions for pure PET (fig.8). In order to emphasize these differences, we have represented in fig.14 the evolution of $\Delta\epsilon$ and $F_{max}$ with crystallinity during the SWD isothermal crystallization experiment at T=96°C for both PET and PET/PEN 1:1 by weight with $f_{TEN}$ =11%. The crystallinity values for the PET/PEN blend have been corrected by the weight concentration. Both $\Delta\epsilon$

and $F_{max}$ have been normalized to their initial values. It is worth to mention that we are dealing here with the region of low level of crystallinity, $X_c$ <10%, where PET still exhibits a single $\alpha$-relaxation (Fig.8). In this crystallization regime the segmental dynamics of the PET/PEN blend seems to be more affected by the crystal development as reflected by the stronger reduction of the $F_{max}$ values as compared with those of pure PET. In contrast, the blend shows a weaker decrease of $\Delta\epsilon$ with crystallinity than pure PET. Considering that the PET domains in the blend are embedded within the glassy PEN matrix then the observed differences in the evolution of the dynamics with the crystallinity can be attributed to a confinement effect. Firstly, the formation of T-E-N linkages located in the interface among PET and PEN domains in the PET/PEN blend with $f_{TEN}$ =11% provokes a slowing down the PET segmental dynamics, as compared to that of pure PET, due to a pinning effect. Secondly, in pure PET the observed strong reduction of the mobile material characterized by the decrease of $\Delta\epsilon$ has been attributed to the formation of an immobilized amorphous phase (RAP) additionally to the crystalline phase. The RAP in PET has been suggested to be assigned to the intra-lamellar amorphous phase where molecular mobility is strongly inhibited [35]. The weaker reduction of $\Delta\epsilon$ of the PET/PEN blend with $f_{TEN}$ =11% can be interpreted as due to a lower probability of lamellar stack formation due to the fact that lamellar crystals are forced to grow within a confined space. A smaller population of lamellar stacks in the blend should imply a smaller amount of RAP, as compared with pure PET, and therefore a weaker reduction of $\Delta\epsilon$. For example, in the restricted geometry imposed in thin films of the order of $\approx$ 102 nm in thickness, it was shown that PET presents isolated lamellae because spherulitic growth is severely limited [51]. Thirdly, pure PET, during its initial period of crystallization, $X_c$ <10%, slightly changes the average segmental mobility in the amorphous phase as reflected by the moderate variation observed in $F_{max}$. This is proposed to be so because, as previously discussed, the $\alpha$-relaxation mainly originates in the inter-lamellar stacks of amorphous regions. The stronger decrease of $F_{max}$ for the PET/PEN blend with $f_{TEN}$=11% can be interpreted by considering that lamellar crystals forced to grow within a confined space are more likely to affect the dynamics of the remaining amorphous phase due to a more effective filling of the available space.

## 6 Conclusions

The simultaneous combination of techniques probing structure (WAXS and SAXS ) with relaxation methods, detecting modifications of the amorphous phase dynamics (dielectric spectroscopy), can be helpful in order to obtain complementary information about cold crystallization processes in aromatic polyesters. In this review we have presented results which are consistent with a heterogeneous morphology in which lamellar stacks are separated by broad

amorphous regions. There are two clearly differentiated regimes of crystallization. Firstly, a primary regime where lamellar stacks are formed. The amorphous phase within the stacks (intra lamellar amorphous phase) seems to be highly constrained and can be assigned to the rigid amorphous phase (RAP). Secondly, a secondary regime in which either isolated lamella or defective lamellar stacks grow in broad amorphous regions located between the stacks. During the second regime of crystallization the rate of RAP formation is reduced. The extension of this kind of experiments to a greater variety of polymers seems to be highly desirable in order to improve our knowledge about polymer crystallization.

## Acknowledgements

We would like to express our gratitude to our colleagues C. Alvarez, Z. Denchev, D.R. Rueda, S.S. Funari, M. Jiménez-Ruiz and F.J. Baltá-Calleja whose support contributed to many of the results presented here. Also we are indebted to MCYT from Spain (grant MAT2005-01768) and to the European Community(EC) ( MERG-CT-2004-511908 and MERG-CT-2004-505674) for generous support of this investigation. The experiments at HASYLAB(Hamburg, Germany) were supported by the European Community - Research Infrastructure Action under the FP6 "Structuring the European Research Area" Programme (through the Integrated Infrastructure Initiative "Integrating Activity on Synchrotron and Free Electron Laser Science".).

## References

[1] E.J. Donth, *Relaxation and Thermodynamics in Polymers.* (Akademie Verlag Berlin, 1992).
[2] K.F. Kelton, *Crystal Nucleation in Liquids and Glasses. Solid State Physics 45* . (Academic Press New York, 1991).
[3] G. Strobl, *The Physics of Polymers* ( Springer Berlin, 1996).
[4] C. Talon , F.J. Bermejo ,C. Cabrillo , G.J. Cuello , M.A. Gonzalez , J.W. Richardson , A. Criado , M.A. Ramos , S. Vieira , F.L. Cumbrera, L.M. Gonzalez : Phys. Rev. Letters 88,115506 (2002)
[5] H.C. Semmelhack , P. Esquinazi: Physica B, 254, 14(1998).
[6] M. Jimenez-Ruiz , T.A. Ezquerra , I. Sics , M.T. Fernandez-Diaz: Applied Phys. A-Mat.Sci.& Process., 74, S543 ( 2002).
[7] A. Sanz, M. Jimenez-Ruiz, A. Nogales, D.M.Y. Marero, T.A.Ezquerra: Phys. Rev. Letters 93, 015503 (2004).
[8] M. Bark and H. G. Zachmann: Acta Polymerica 44, 18 (1993).
[9] E. Eckstein , J. Qian , T. Thurn-Albrecht, W. Steffen and E.W. Fischer: J. of Chem. Phys. **113**, 4751 (2000).

[10] I. Šics , A. Nogales , T.A. Ezquerra , Z. Denchev F.J. Baltá-Calleja ,A. Meyer , R.Döhrmann : Rev. of Sci. Instrum., 71, 1733(2000).
[11] M. Jimenez-Ruiz , A. Sanz ,A. Nogales ,T.A. Ezquerra : Rev. of Sci. Instrum., 76, 043901(2005).
[12] F. Kremer, A. Schönhals (Eds.) *Broadband Dielectric Spectroscopy*, (Springer Berlin, 2003).
[13] G. Williams:, G. Adv. Polym. Sci. 33, 59 (1979).
[14] J.C. Coburn, R.H. Boyd:. Macromolecules 19, 2238 (1986).
[15] T.A. Ezquerra, J. Majszczyk, F.J. Baltá-Calleja, E. López-Cabarcos, K.H. Gardner, B.S. Hsiao, Phys. Rev. B 50, 6023 (1994).
[16] J. Dobbertin , A. Hensel, C.J. Shick: Thermal Anal. 47, 1027 (1996).
[17] T.A. Ezquerra and A. Nogales in *Lecture Notes in Physics: Polymer Crystallization: Observations, Concepts and Interpretation* ed. by J.-U. Sommer, G. Reiter ( Springer Berlin, 2003) pp.275.
[18] P. Hedvig: *Dielectric Spectroscopy of Polymers* ( Bristol: Adam Hilger Ltd, 1997).
[19] N.G. McCrum, B.E. Read, G. Williams: *Anelastic and Dielectric Effects in Polymeric Solids* (Dover, New York, 1991, Original Issue John Wiley, London 1967).
[20] A.R. Blythe: *Electrical Properties of Polymers* (Cambridge: Cambridge University Press, 1979).
[21] F.J. Baltá-Calleja and C.G. Vonk , *X-ray Scattering of Synthetic Polymers* (Elsevier, Amsterdam, 1989).
[22] K. Fukao, Y. Miyamoto: Phys. Rev. Lett. 79,4613 (1997).
[23] A. Wurm , R. Soliman , J.G.P. Goossens , W. Bras , C. Schick:J. of Non-Crystalline Solids 351(33-36), 2773 (2005).
[24] *Handbook of Thermoplastic Polyesters* ed. by S. Fakirov ( Wiley-VCH: Weinheim , 2002).
[25] G. Groeninckx , H. Reynaers , H. Berghmans, G.Smets: J. Polym. Sci. Polym. Phys.18, 3111 (1980)
[26] S. Monserrat , P. Corts: J. of Mater. Sci. 30, 1790 (1995)
[27] J.F. Medellin-Rodriguez, P. J. Phillips ,J. S. Lin: Macromolecules. 29, 7491 (1996).
[28] N. M. Alves , J. F.Mano , E. Balaguer , J. M. Meseguer Dueas, J. L. Gmez Ribelles: Macromolecules. 43, 4111 (2002).
[29] R. Androsch, B. Wunderlich: Polymer. 46, 12556 (2005).
[30] A.M. Jonas , T.P. Russell , D.Y. Yoon: Colloid&Polymer Sci. 272, 1344 (1994).
[31] C. Santa Cruz , N. Stribeck,H.G. Zachmann , F.J. Balt-Calleja: Macromolecules. 24, 5980 (1991).
[32] Z.G. Wang ,B.S. Hsiao ,B.X. Fu ,L. Liu ,F. Yeh ,B.B. Sauer ,H. Chang ,J.M. Schultz: Polymer. 41, 1791 (2000)
[33] D.A. Ivanov, Z.Amalou, S.N. Magonov: Macromolecules. 34, 8944 (2001).
[34] C. Schick , E. Donth: Physica Scripta 43, 423 (1991).

[35] C. Alvarez, I. Sics,A. Nogales, Z. Denchev, S.S. Funari, T.A. Ezquerra: Polymer. 45, 3953 (2004).
[36] S. Havriliak and S. Negami: Polymer 8, 161 (1967).
[37] S.P. Bravard, R.H. Boyd: Macromolecules. 36, 741(2003).
[38] A. Sanz, A. Nogales, T.A. Ezquerra, N. Lotti, L. Finelli. Phys. Rev. E: 70, 021502 (2004).
[39] D. J. Blundell and B. N. Osborn: Polymer 24, 953 (1983).
[40] S.Z.D. Cheng , Z. Q. Wu ,B. Wunderlich: Macromolecules. 20 ,2802 (1987).
[41] M. Okamoto, T. Kotaka: Polymer: 38, 1357 (1997).
[42] Z. Denchev, T.A. Ezquerra, A. Nogales, I. Šics, C. Alvarez, G. Broza, K. Schulte: J. Polym. Sci.: Part B: Polym. Phys. 40, 2570 (2002).
[43] J.F. Mano, Z. Denchev, A. Nogales, M. Bruix, T.A. Ezquerra: Macromol. Mater. Eng. 288, 778 (2003).
[44] G. Reiter, G. Catelein,J-U. Sommer: Phys. Rev. Letters. 87, 226101 (2001)
[45] C. Alvarez, A. Nogales, M.C. Garca-Gutirrez, A. Sanz, Z. Denchev, S.S. Funari, M. Bruix, T.A. Ezquerra:Eur. Phys. J. E. 18, 459 (2005).
[46] A. Nogales, Z. Denchev, I. Šics, T. A. Ezquerra: Macromolecules. 33(25), 9367 (2000).
[47] J. Lin, S. Shenogin , S. Nazarenko: Polymer. 43,4733 (2002).
[48] D.A. Ivanov , T. Pop , D.Y. Yoon , A.M. Jonas: Macromolecules. 35, 9813 (2002).
[49] A. Sanz, A. Nogales,T.A. Ezquerra, N. Lotti, A. Munari, S.S. Funari: Polymer. In Press(2006).
[50] B. Lee, T.J. Shin, S.W. Lee, J. Yoon, J. Kim, M. Ree: Macromolecules. 37,4174 (2004).
[51] H.G. Haubruge, R. Daussin, A.M. Jonas, R. Legras: Polymer. 44, 4733 (2003).

# Index